Design of Vaterite Nanoparticles for Controlled Delivery of Active Immunotherapeutic Proteins

Nelemans, Levi Collin; Choukrani, Ghizlane; Ustyanovska-Avtenyuk, Natasha; Wiersma, Valerie R.; Dähne, Lars; Bremer, Edwin

Published in:
Particle and Particle Systems Characterization

DOI:
10.1002/ppsc.202300153

RESEARCH ARTICLE

Particle & Particle Systems Characterization
www.particle-journal.com

Design of Vaterite Nanoparticles for Controlled Delivery of Active Immunotherapeutic Proteins

*Levi Collin Nelemans, Ghizlane Choukrani, Natasha Ustyanovska-Avtenyuk, Valerie R Wiersma, Lars Dähne, and Edwin Bremer**

Despite clinical advances in immunotherapy, still many therapeutics cause dose-limiting (auto)immune-mediated toxicities. Nanoparticle-based drug delivery systems (DDS) can improve cancer immunotherapy through site-specific delivery and controlled release of immunotherapeutics in the tumor microenvironment (TME). However, DDS face several challenges, including unspecific release. To address this, vaterite nanoparticles (VNPs) that selectively release immunotherapeutic proteins at low pH conditions find in the TME, are established previously. In the current study, these VNPs are further modified for active targeting without affecting the loaded protein activity, exemplified with Tumor Necrosis Factor α (TNF). Specifically, VNPs are coated with gelatin, a matrix-metalloprotease sensitive polymer which provides functional groups for further conjugation. Subsequently, streptavidin is covalently linked to the gelatin shell by amine-epoxy chemistry, enabling coupling of any biotinylated ligand. Exemplified by biotinylated cetuximab and rituximab, targeted VNPs selectively bind to cells expressing epidermal growth factor receptor (EGFR) or CD20, respectively. Importantly, TNF remains functionally active after the modification steps, as VNP treatment increased ICAM-1 expression on FaDu cells and activated NFκB signaling in a Jurkat.NFκB-luciferase cell line model. In conclusion, a targetable vaterite-based DDS is produced that allows for easy surface modification with any biotinylated ligand that may find broad applications in tumor-selective immunotherapy.

1. Introduction

Immunotherapy with immune checkpoint inhibitors (ICIs) that (re)activate tumor-directed T cell response have achieved impressive success in the treatment of different types of cancer.[1,2] Yet, ICIs and other immunotherapies have limited intrinsic selectivity for cancer and can ubiquitously reactivate immunity, leading to sometimes severe immune-related side-effects.[3] For example, the clinically successful ICIs targeting programmed cell death protein 1 (PD-1), its ligand PD-L1, or cytotoxic T lymphocyte antigen-4 (CTLA-4), can in addition to the desired reactivation of anti-tumor T cell activity, also trigger on-target yet off-tumor gastrointestinal and endocrine toxicities and/or organ-specific inflammatory side effects (e.g., colitis, hepatitis, pneumonitis).[4,5] Similarly, immune checkpoint inhibition of innate checkpoint CD47 can induce anemia, which can be so severe it can lead to death.[6] Immunotherapeutic cytokines suffer from similar drawbacks, for example IL-2 treatment can lead to severe pulmonary edema.[7] Finally, the clinical use of tumor necrosis factor α (TNF) has been constrained due to inflammatory side-effects including dose-limiting hypotension, hepatotoxicity, hemorrhage, and intravascular thrombosis.[8,9] Consequently, TNF can only be administered locally, such as isolated limb or liver perfusion.[10,11] Thus, there is an almost universal need for strategies that limit off-tumor activity of cancer immunotherapy.

Nanomedicine is a new strategy that has been applied to the field of immunotherapy in recent years.[12–14] Here, active immunotherapeutic drugs are encapsulated inside nanoparticles, which shield the drug and prevent systemic exposure, while providing opportunities for selective release at the tumor microenvironment (TME). The physicochemical properties of nanoparticles such as size, shape, composition, and surface properties have a great impact on their interaction with the biological environment. Therefore, a wide variety of organic and inorganic nanoparticles have been engineered for specific drug delivery applications.[15] However, there are major design challenges associated with encapsulation and delivery of bioactive proteins including, but not limited to, achieving optimal drug

L. C. Nelemans, G. Choukrani, N. Ustyanovska-Avtenyuk, V. R Wiersma, E. Bremer
Department of Hematology
University Medical Center Groningen (UMCG)
University of Groningen
Hanzeplein 1, Groningen 9713 GZ, The Netherlands
E-mail: e.bremer@umcg.nl
L. Dähne
Surflay Nanotec GmbH
Max-Planck-Straße 3, 12489 Berlin, Germany

The ORCID identification number(s) for the author(s) of this article can be found under https://doi.org/10.1002/ppsc.202300153

DOI: 10.1002/ppsc.202300153

loading, ensuring protein stability, and preventing unspecific drug release. These challenges require new design strategies for protein-based drug delivery systems (DDS).

Vaterite, a polymorph of calcium carbonate ($CaCO_3$), has gained considerable attention as a DDS for small and large molecules.[16–19] We recently established vaterite nanoparticles (VNPs) as an efficient protein drug carrier that can selectively release its contents at tumor microenvironmental conditions.[20] VNPs can be simply and rapidly synthesized by coprecipitation of Ca^{2+} and CO_3^{2+} in the presence of a surfactant such as ethylene glycol to control the particle size.[21] As detailed in our previous study, controlling the coprecipitation pH by using different precursors further preserved the functional activity of the protein to be loaded, while increasing the loading efficiency. Interestingly, VNPs dissolve faster in acidic pH conditions in aqueous solutions, a property that can be exploited for controlled drug release in the TME due to a low tumor microenvironmental pH. Indeed, using an in-house developed system mimicking tumor microenvironmental pH and blood flow conditions, VNP dissolution was increased at acidic pH conditions, leading to sustained release of over 80% of the loaded bioactive protein within 2 hours compared to less than 20% at physiological conditions.[20]

In this study, VNPs were further developed as a DDS for hydrophilic immunotherapeutic protein-based drugs with active targeting capabilities. Hereto, the surface of the VNPs were first coated with gelatin, whereupon streptavidin was conjugated to the gelatin shell while retaining activity of the pre-loaded therapeutic protein. Subsequently, biotinylated ligands to any target antigen of choice can be employed for targeted delivery of the DDS. Proof-of-concept for this system was generated using the clinical antibodies rituximab (RTX)(anti-CD20) and cetuximab (CTX)(anti-epidermal growth factor receptor (EGFR)), with clear CD20 or EGFR-dependent accretion of targeted VNPs to the surface of cancer cells. Importantly, the therapeutic protein TNF, which was encapsulated in the DDS, was successfully released from the particles and retained functional activity, with a TNF-induced increase in intercellular adhesion molecule 1 (ICAM-1) expression on cancer cells and activation of nuclear factor kappa B (NFκB) signaling in Jurkat NFκB reporter cells. The here presented functionalization strategy of VNPs as a DDS for hydrophilic protein delivery may find broad applications in cancer-selective immunotherapy.

2. Results

2.1. TNF-Loaded Vaterite Nanoparticles can be Successfully Coated with Gelatin while Retaining Bioactivity upon Release

VNPs were generated as previously described[21] and had an average size of ≈400 nm with a homogeneous size distribution (**Figure 1A**) and high porosity as evaluated by Scanning Electron Microscopy (Figure 1, inset). As previously demonstrated, the porosity of VNPs allow for a high loading efficiency of TNF.[20] Indeed, loading of the negatively charged TNF reduced the surface charge (zeta potential) of VNPs from +16 to -20 mV (Figure 1B) with a loading capacity of 4.3 ± 0.9%.

Further, to increase aqueous stability, protect the loaded TNF, and provide functional groups, VNPs were coated with a shell of gelatin type A (GelA) or B (GelB) through electrostatic attraction, yielding VNP-GelA or VNP-GelB, respectively. Successful coating of VNPs was verified by confocal microscopy using Rhodamine-labeled GelB, with a gelatin shell being detected (Figure 1C).

Release of functionally active TNF from VNPs is critical for the intended mode-of-action of tumor-localized release of immunotherapeutics. Using flow cytometry, a significant ≈4-fold increase of ICAM-1 expression was detected on FaDu cells upon overnight treatment with TNF-loaded VNPs with or without GelA or GelB coating (Figure 1D,E). Of note, ICAM-1 is a protein that is upregulated on endothelial and epithelial cells upon stimulation with TNF.[22] Presumably, some TNF was lost during the coating, as ICAM-1 expression after GelA and GelB treatment was slightly lower than treatment with uncoated VNPs (Figure 1D,E). Supernatant from overnight pre-released VNPs at pH 7.4 and 5.0, induced significantly less ICAM-1 expression compared to directly added VNPs for uncoated and GelB-coated VNPs (Figure 1F,G), but was not significant for GelA-coated VNPs (Figure 1H). At pH 7.4, ICAM-1 expression was almost comparable to untreated FaDu cells, as supernatant from uncoated and GelB-coated VNPs only caused an ICAM-1 fold change of 1.6 and 1.3, respectively (Figure 1F,G). This data suggests minimal TNF release at pH 7.4. Supernatant of pre-released VNPs at pH 5.0 increased ICAM-1 expression in the case of the uncoated particles, although not significantly (1.6 to 2.7 fold (Figure 1F)). On the other hand, ICAM-1 expression on FaDu treated with supernatant from GelB-coated or GelA-coated vaterite (VNP-TNF-GelB and VNP-TNF-GelA) was comparable at both pH conditions (1.4 to 1.6 and 2.9 to 2.7 for VNP-TNF-GelB and VNP-TNF-GelA, respectively; Figure 1G,H). As GelB-coated VNPs acted in a similar manner as uncoated VNPs at pH 7.4 and prevented more TNF leakage from the particle compared to GelA coating, subsequent experiments were continued with GelB.

Overnight exposure of VNP-GelB to FaDu cells proved not toxic, as FaDu cell viability determined by Annexin V/PI staining (Figure 1I) and MTS assay (Figure 1J) remained similar to control. Interestingly, whereas the viability of the VNP-GelB exposed FaDu cells was similar to control, flow cytometry did reveal an increase in the side scatter of VNP-GelB exposed FaDu cells, suggesting an increase in granularity of the cells (Figure S1A, Supporting Information). Therefore, confocal microscopy was used to evaluate potential VNP-GelB uptake in FaDu cells after overnight incubation. As demonstrated in an orthogonal view (X, Y, Z slice) in Figure 1K (left panel), VNP-GelB particles (orange) were accumulating inside a FaDu cell that was stained for surface marker CD47 (green), with white arrows indicating the same particle in either the X, Y or Z plane within the FaDu cell. Using a maximum intensity projection of the same image (Figure 1K, right panel), it is evident that particles localized inside FaDu cells, whereas some particles were also detected outside (blue arrows). In conclusion, VNPs were successfully loaded with TNF, coated with gelatin and were not toxic to FaDu cells. Furthermore, overnight exposure to VNP-GelB caused particle uptake by FaDu.

To confirm functionality of the TNF released from VNPs, a Jurkat.NFκB.luciferase reporter cell line was treated with intact VNP-TNF or supernatant from overnight pre-released VNP-TNF, which yielded an increase in luminescence of ≈20x or ≈30x, respectively (Figure 1L). In contrast, treatment with empty VNPs did not increase luminescence. Notably, treatment with

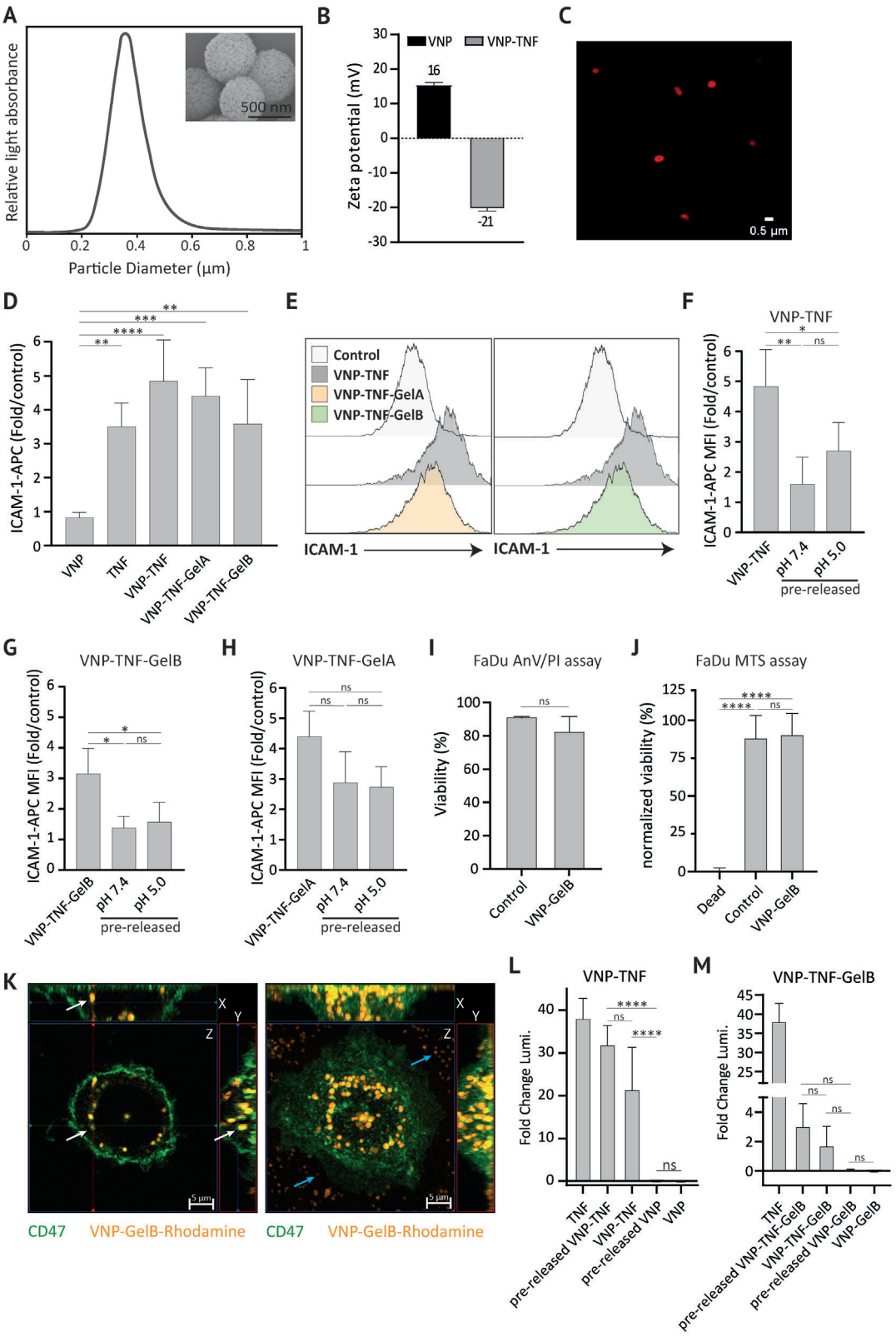

Figure 1. A) Disc centrifuge (CPS) measurement with size distribution of produced VNPs. Inset: Field Emission Scanning Electron Microscopy (FESEM) image of VNP. The scale bar denotes 500 nm B) Zeta potential of empty and TNF loaded VNPs. C) Confocal image of Gelatin-B-Rhodamine coated VNPs. The scale bar denotes 500 nm D) ICAM-1 expression on FaDu cells after overnight treatment with TNF loaded VNPs with and without Gel-A/Gel-B coating. E) as in (D) but with representative flow cytometry histograms. ICAM-1 expression on FaDu after overnight treatment with whole particle

GelB-coated VNPs also increased luminescence, but only by a factor three for pre-released VNP-TNF-GelB and a factor two for intact VNP-TNF-GelB (Figure 1M). Again, treatment with empty VNP-GelB particles lacking TNF did not increase luminescence. Thus, both VNP-TNF and VNP-TNF-GelB activated the NFκB pathway in the Jurkat.NFκB.luc report cell line, although a near ten times fold reduction in activity was detected between GelB-coated and non-coated particles, possibly due to loss of TNF during the coating procedure.

2.2. Streptavidin was Conjugated to Gelatin-Coated VNPs using Amine-Epoxy Chemistry

To enable facile coupling of any biotinylated ligand to the surface of VNP, streptavidin was conjugated to the VNP-GelB surface using an amine-epoxy "click" reaction, using various cross-linkers (**Figure** 2A). All the used cross-linkers allowed for successful conjugation of streptavidin-FITC to the particle surface (Figure 2B), with no autofluorescence emitted from the cross-linked gelatin (Figure S1B, Supporting Information). Importantly, TNF that was pre-loaded into VNP-GelB retained functional activity in streptavidin-functionalized particles generated with amine-epoxy conjugated cross-linkers, whereas a slight decrease in TNF activity was observed in the glutaraldehyde cross-linked group (Figure 2C). Thus, streptavidin coupling to vaterite via the amine-epoxy reaction did not negatively impact TNF activity with exception of glutaraldehyde cross-linking.

To verify the functional activity of streptavidin after cross-linking, CD20-positive Daudi cells were pretreated with biotinylated RTX (anti-CD20), and subsequently incubated with streptavidin coated VNPs (VNP-GelB-Strep) (Figure 2D). All the particles that were cross-linked with streptavidin using amine-epoxy chemistry bound to the surface of Daudi cells only when pre-incubated with RTX-biotin (Figure 2E). In contrast, the particles that used glutaraldehyde as a cross-linker did not bind to the cell surface (Figure 2E). Biotinylation did not affect the binding of the antibody, as exemplified by biolayer interferometry analysis of CTX-biotin to EGFR (Figure S1C, Supporting Information). Active targeting was further verified with nanoparticles conjugated with either biotinylated CTX (VNP-CTX) or biotinylated RTX (VNP-RTX), with VNP-CTX only binding to the surface of EGFR-positive FaDu and not EGFR-negative Daudi cells (**Figure** 3A,B). Reversely, VNP-RTX bound to the surface of Daudi cells and not CD20-negative FaDu cells (Figure 3C,D) as well as a panel of six diffuse large B-cell lymphoma cell lines (Figure S1D–I, Supporting Information), except for two cell lines, OCI-LY3 and U2932 (Figure S1J,K, Supporting Information). Again, in a mixed population of FaDu and Daudi cells, VNP-CTX specifically bound to FaDu but not to Daudi as depicted by flow cytometry analysis (Figure 3E,F).

2.3. EGFR-Targeted VNPs Enhance Cellular Uptake by FaDu Cells

Depending on the target antigen used for VNP delivery, cellular uptake may be triggered. In this respect, EGFR is known to be a rapidly internalizing antigen whereas CD20 is a tetraspanin that only slowly internalizes.[23] In line with these characteristics, VNP-CTX particles (green) were rapidly taken up and accumulated inside FaDu cells (surface marker CD47, red)(Figure 3G). Notably, the uptake of VNP-CTX by FaDu cells was significantly higher than that of VNP, with VNP-CTX being taken up twice as much when exposed to FaDu cells compared to VNP-RTX or VNP (Figure 3H,I). In conclusion, the VNPs that were developed here can be used for active targeting by conjugation of any biotinylated marker to its surface.

2.4. Functionalization Steps of VNPs Lead to Loss of Loaded TNF

Importantly, ICAM-1 expression on FaDu was increased by two-fold when treated with VNP-CTX, highlighting that TNF activity was retained in the DDS after all functionalization steps (**Figure** 4A,B). Furthermore, the ICAM-1 fold increase did not significantly change when FaDu was treated with VNP-TNF-GelB, VNP-TNF-GelB-Strep, or VNP-TNF-CTX, indicating functional TNF activity (Figure 4A,B).

Whereas the TNF in the fully functionalized VNPs remained functionally active based on the ICAM-1 assay, the more sensitive Jurkat.NFκB.luciferase reporter assay demonstrated a significant decrease in luminescence between VNP-TNF, VNP-TNF-GelB and VNP-TNF-GelB-Strep upon treatment with overnight released supernatant (Figure 4C). In contrast, there was no significant difference between VNP-TNF-GelB-Strep and VNP-RTX or VNP-CTX particles. Thus, the coating steps of VNP-TNF with GelB and streptavidin might induce loss of TNF. Indeed, the total functional TNF weight inside the VNPs was decreased after GelB and streptavidin coating, using ELISA (Figure 4D). Coating with GelB and streptavidin led to a loss of ≈80% of TNF, compared to the prior step (Figure 4E) and the attachment of CTX or RTX led to a loss of 20–40% of TNF.

Therefore, although the employed streptavidin-biotin system for the functionalization of targeting ligands to VNP is simple and enables easy coupling of targeting ligands and preservation of functional activity of therapeutic proteins, it currently suffers from premature loss of therapeutic protein in the modification steps.

3. Discussion

In this study, we further developed a VNP-based DDS for therapeutic protein delivery, by modifying the surface of VNPs for easy

(VNP name) or the supernatant (pre-released followed by pH) of F) VNP-TNF, G) VNP-TNF-GelB, H) VNP-TNF-GelA dissolved at pH 7.4 or 5.0. Viability of FaDu after overnight treatment with VNP-GelB as measured by I) annexinV/PI staining and J) MTS assay. K) Live cell confocal images showing an orthogonal view (X, Y, Z slice) of FaDu cells after overnight incubation with VNP-Gel-B-Rhodamine. The scale bar denotes 5 µm. Luminescence fold change measured after 6 h treatment of a Jurkat.NFκB.luc reporter cell line (activated by TNF) with whole nanoparticle or supernatant from overnight pre-released L) VNP-TNF and M) VNP-TNF-GelB. *Abbreviations: vaterite nanoparticles (VNPs); VNP loaded with tumor necrosis factor alpha (TNF) (VNP-TNF); VNP-TNF coated with gelatin A (VNP-TNF-GelA); VNP-TNF coated with gelatin B (VNP-TNF-GelB); VNP coated with GelB (VNP-GelB); VNP coated with labeled Gelatin B-rhodamine (VNP-GelB-Rhodamine); Intercellular Adhesion Molecule 1 (ICAM-1).*

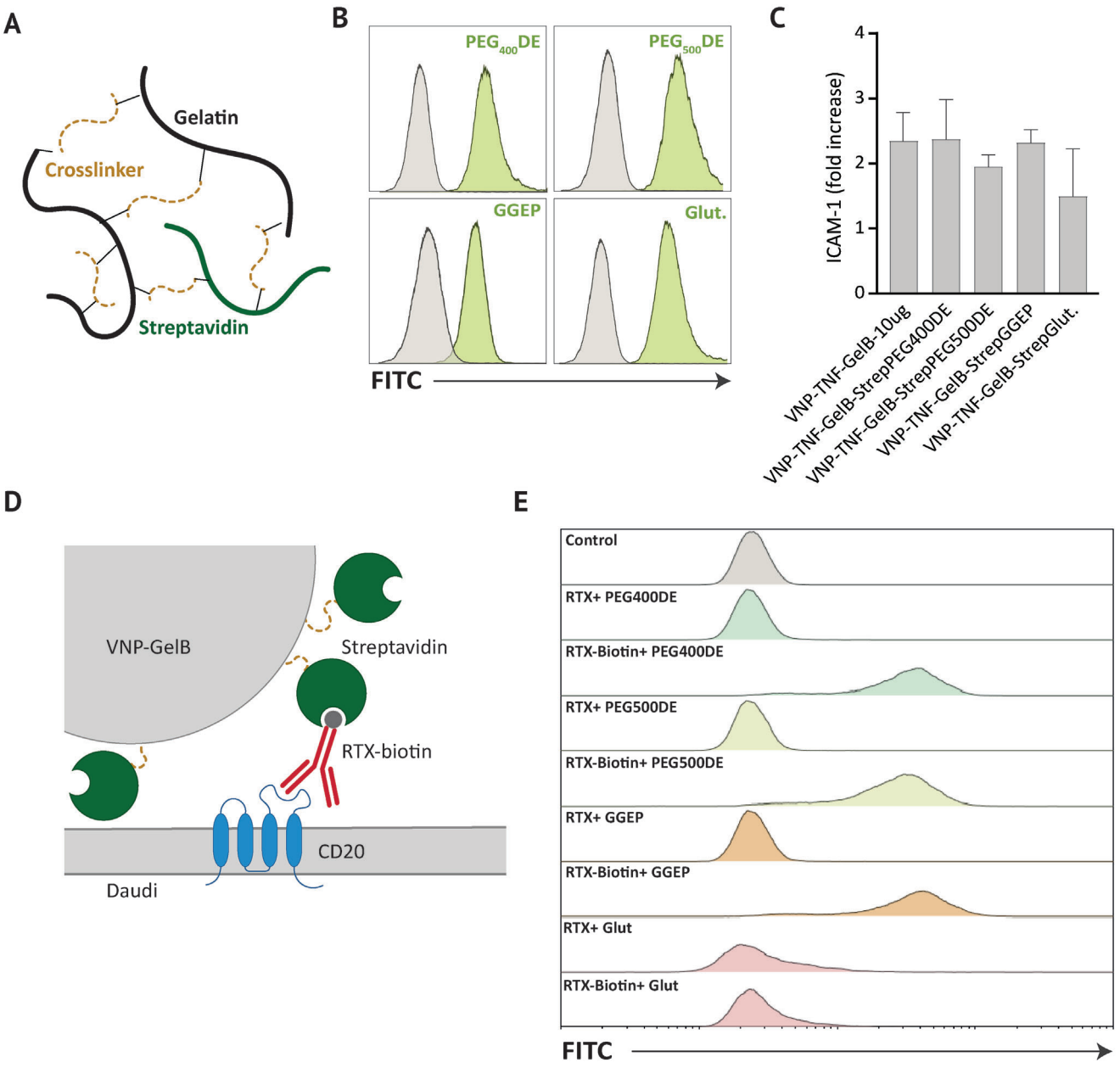

Figure 2. A) Schematic illustration of Gelatin cross-linking with streptavidin. B) Binding of streptavidin-FITC to Gel-B coating on VNPs using different cross-linkers as measured by flow cytometry, $PEG_{400}DE$: Poly(Ethylene Glycol) (400) Diglycidyl Ether, $PEG_{500}DE$: Poly(Ethylene Glycol) (500) Diglycidyl Ether, GGEP: Glycidyl Glycerol-Ether, Polyfunctional, Glut: Glutaraldehyde. C) Flow cytometry analysis of fold increase of ICAM-1 expression on FaDu cells after overnight treatment with streptavidin bound VNP-TNF with different cross-linkers. D) Schematic illustration of proposed VNP-Strep binding to surface bound RTX-biotin (rituximab, anti-CD20) to CD20 on Daudi (EGFR-/CD20+). E) Flow cytometry histograms of binding of VNP-strep-FITC synthesized with different cross-linkers (PEG400DE, PEG500DE, GGEP, Glut) to RTX-biotin on the surface of Daudi (EGFR-/CD20+). *Abbreviations: vaterite nanoparticles (VNPs); VNP loaded with tumor necrosis factor alpha (TNF) (VNP-TNF); VNP-TNF coated with gelatin B (VNP-TNF-GelB); VNP coated with GelB (VNP-GelB); VNP-TNF-GelB with covalently attached streptavidin (VNP-TNF-GelB-Strep).*

and efficient coupling of any biotinylated molecule of interest (e.g., targeting ligands). This was achieved by coating VNPs with the biocompatible polymer gelatin and the subsequent coupling of streptavidin to the gelatin shell with amine-epoxy chemistry. Furthermore, the DDS could be successfully targeted to EGFR and CD20 expressing cell lines by coupling respectively biotinylated CTX and RTX to -VNP-Strep. This conjugation strategy retained the functional activity of the loaded immunotherapeutic protein TNF as demonstrated by the upregulation of ICAM-1 on the surface of FaDu and activation of NFκB in the reporter cell line Jurkat.NFκB.luciferase.

As demonstrated by us[20] and others,[17,19,21] VNPs can be successfully loaded with a variety of hydrophilic proteins with different size and charge characteristics. The high loading efficiency

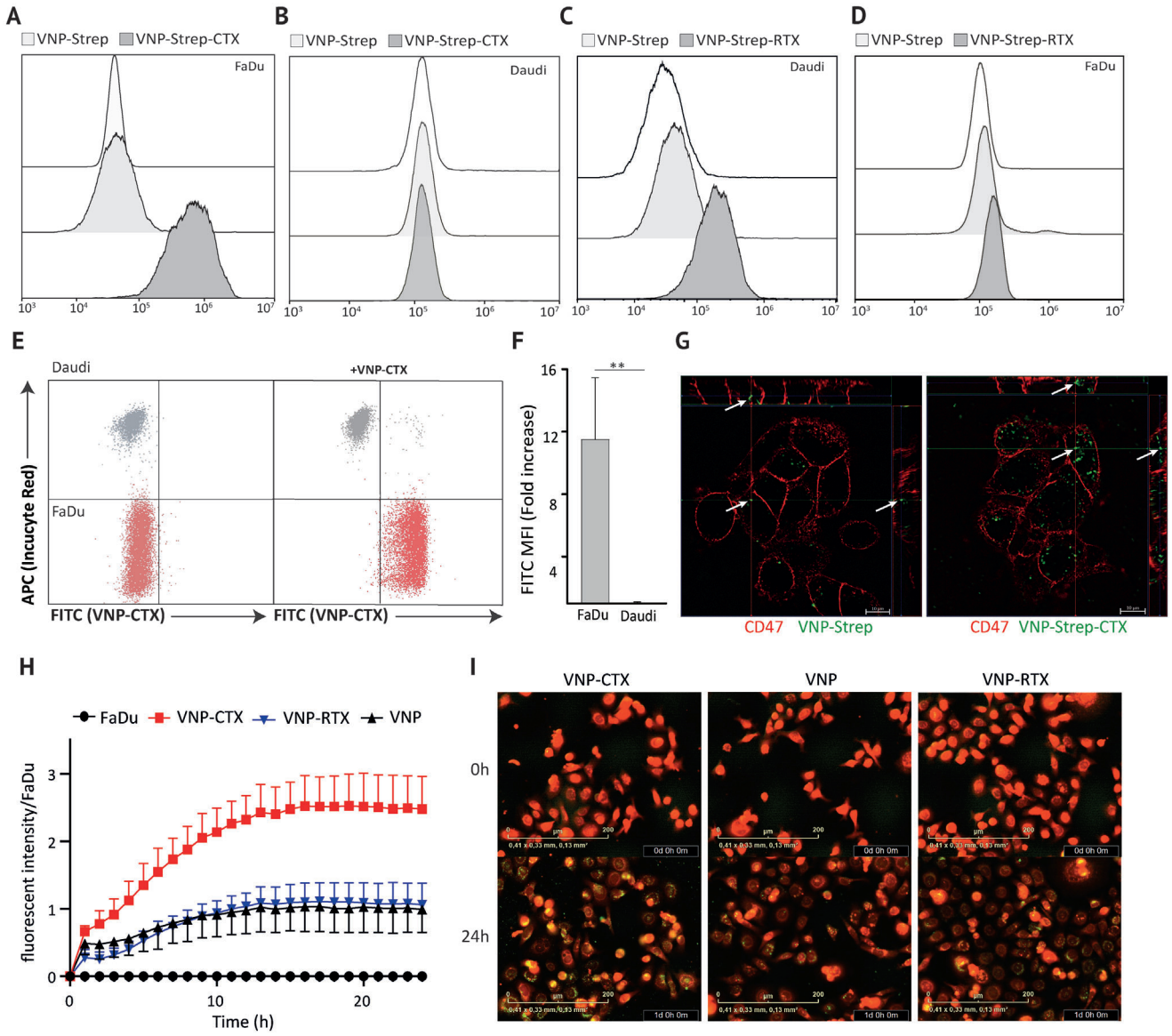

Figure 3. Flow cytometry histograms of binding of VNP-Strep-CTX (anti-EGFR) to the surface of A) FaDu (EGFR+/CD20-), B) Daudi (EGFR-/CD20+). Binding of VNP-RTX (anti-CD20) to the surface of C) Daudi, D) FaDu. E) Flow cytometry dot plot and F) calculated fold increase of binding of VNP-CTX in a mix culture of Daudi and FaDu. G) Confocal images showing an orthogonal view (X, Y, Z slice) of overnight uptake of VNP-GelB-Strep and VNP-GelB-Strep-CTX (anti-EGFR) by FaDu (EGFR+/CD20-) cells. White arrows indicate the same particle in X, Y and Z slice. The scale bar denotes 10 µm. H) Quantification of VNP, VNP-RTX (anti-CD20), and VNP-CTX (anti-EGFR) uptake by FaDu (EGFR+/CD20-) every hour up to 24 h using Incucyte S3. I) Representative images as in (H) at t = 0 and t = 24 h showing FaDu (EGFR+/CD20-) (in Red (Incucyte Red) and VNP in green (FITC). The scale bar denotes 200 µm. *Abbreviations: vaterite nanoparticles coated with gelatin B with covalently attached streptavidin (VNP-Strep); VNP-Strep with biotinylated cetuximab (VNP-Strep-CTX); VNP-Strep with biotinylated rituximab (VNP-Strep-RTX).*

is due to the high porosity of vaterite particles, which provides a large surface area for the loading of different drug molecules by simple diffusion, while preserving their physicochemical and biological properties.[20]

After loading of TNF to VNP, the surface of the particles was coated with gelatin to which streptavidin was conjugated using amine-epoxy chemistry. Compared to the common cross-linking method with glutaraldehyde, amine-epoxy cross-linking proved to be a better strategy to link macromolecules on the surface of nanoparticles with the therapeutic protein TNF already loaded in the pores. Specifically, the herein employed polyethylene glycol (PEG) terminated glycidyl molecules have a large size and are therefore unlikely to penetrate through the gelatin mesh to the loaded protein compared to small cross-linking molecules such as glutaraldehyde. Indeed, the functional activity of TNF as well as streptavidin was not affected after the reaction, whereas glutaraldehyde cross-linking caused denaturation of streptavidin and a reduction of TNF activity. Epoxy resins are reactive intermediates formed through the epoxide ring-opening cross-linking of macromers such as glycidyl-terminated PEG and

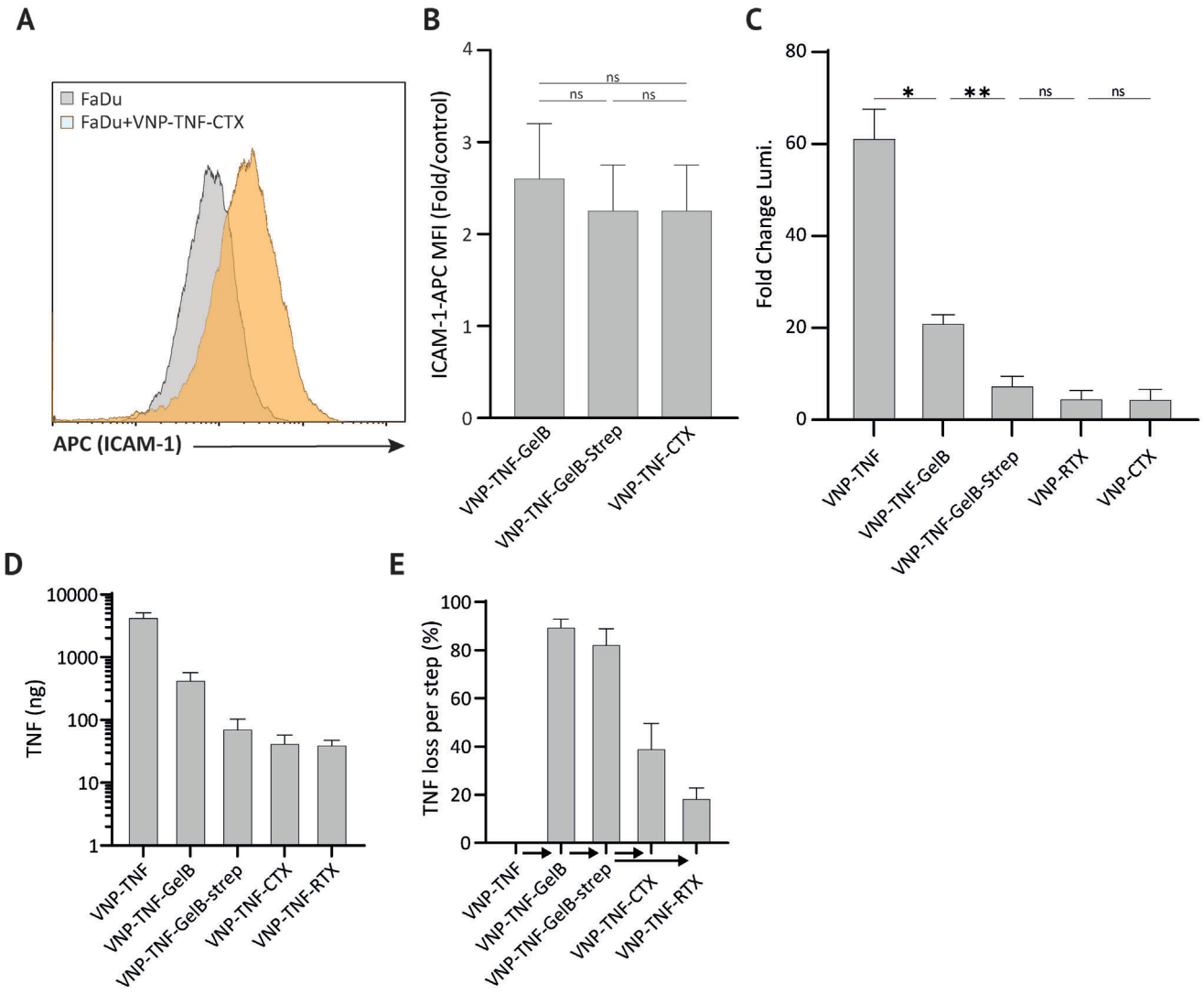

Figure 4. A) Representative histogram of ICAM-1 expression on FaDu (EGFR+/CD20-) after overnight treatment with VNP-TNF-CTX (anti-EGFR) and quantified B) for VNP-TNF-GelB, VNP-TNF-GelB-Strep and VNP-TNF-CTX using flow cytometry. C) Luminescence fold change measured after 6 h treatment of a Jurkat.NFκB.luc reporter cell line (activated by TNF) with supernatant from overnight pre-released VNP-TNF, VNP-TNF-GelB, VNP-TNF-GelB-Strep, VNP-RTX, VNP-CTX. D) Total amount of TNF inside 0.1 mg of VNPs E) Calculated percentile TNF loss after each modification step indicated in figures. *Abbreviations: vaterite nanoparticles (VNP); VNP loaded with tumor necrosis factor alpha (TNF) (VNP-TNF); VNP-TNF coated with gelatin B (VNP-TNF-GelB); VNP-TNF-GelB with covalently attached streptavidin (VNP-TNF-GelB-Strep); VNP-TNF-GelB-Strep with biotinylated cetuximab or rituximab (VNP-CTX or VNP-RTX).*

bisphenol-A–epichlorohydrin polymers.[24,25] Conjugates of proteins with epoxy containing polymers through amine-epoxy reactions have been used for several applications due to their catalyst free nature, and a wide range of epoxy-functionalized supports are commercially available.[26–28] Hence, the epoxy-amine reaction is a safe and easy method to conjugate biomolecules without altering their functional activity.

Our study demonstrated the functional activity of loaded TNF even after GelB and streptavidin coating, as evidenced by ICAM-1 upregulation on FaDu cells. However, TNF loss from the nanoparticles was observed during the modification steps. Minimizing this loss is crucial for future applications. Currently, multiple washing steps are required between each coating step, which could result in VNP dissolution or calcite formation and subsequent TNF release. To reduce the washing steps, especially when only the end product (e.g., VNP-RTX) is needed, TNF loading could be directly followed by GelB coating without washing. Furthermore, the coating steps were not optimized. The negatively charged GelB might compete with TNF for binding on VNP, leading to TNF removal from the VNP' surface. Currently, a 100-fold excess of GelB is used for coating compared to TNF. Hence, enhancing TNF retention could be achieved by reducing the GelB concentration. Additionally, the streptavidin coating process is long (6 hours), which may result in TNF release, VNP dissolution or calcite formation. We have previously shown that 20% of TNF was released in 2 hours at physiological pH.[20] Alternatively, streptavidin could be attached to GelB prior to VNP coating, reducing both time and functionalization steps. However,

further investigation is required to minimize the loss of bioactive protein during manufacturing.

For a prolonged blood circulation of the nanoparticle and active targeting to the tumor, the nanoparticles' surface must be functionalized with specific ligands.[29] The herein employed streptavidin-biotin system provides an easy strategy to conjugate any biotinylated ligand of interest as illustrated by the successful conjugation of CTX and RTX to selectively target EGFR and CD20, respectively. However, clinical application of this system may be restricted as streptavidin is a bacterial protein to which neutralizing antibodies may develop upon injection.[30] Thus, future studies should focus on either modifying streptavidin to a less immunogenic form for clinical use or other strategies should be developed that are as easy as the streptavidin-biotin system but with better tolerability. Indeed, several groups have succeeded in reducing the immunogenicity of streptavidin, although some also reported alterations in the affinity of streptavidin to biotin.[30–32] Another alternative approach to streptavidin-biotin is the use of designed ankyrin repeat proteins (DARPin). DARPins are engineered proteins derived from natural ankyrin repeat proteins, which are well-tolerated in the body.[33] Anti-DARPin antibodies could then directly be conjugated to the VNPs gelatin surface, providing a universal system for the bioconjugation of specific DARPin-conjugated ligands. Although DARPins has been used for several biomedical applications, more studies are needed to fully understand the safety and efficacy of DARPins in nanoparticle-based DDS.[33–35]

As described above, VNP-CTX selectively targeted EGFR-expressing cell lines and were more rapidly internalized then untargeted VNPs. As CTX inhibits tumor growth and metastasis upon binding to EGFR, VNP-CTX could therefore be explored as a therapeutic strategy in itself or in combination with other molecules.[36,37] For instance, the observed rapid internalization could be exploited for the delivery of cytotoxic molecules such as doxorubicin (DOX) or intracellular immunostimulatory reagents such as stimulator of interferon genes (STING) agonists. DOX has been previously encapsulated in VNPs and treatment associated with less off-target toxicity and more intratumoral accumulation than free DOX.[38,39] Whether targeting the VNPs would further enhance the cytotoxic effect induced by DOX, needs to be further investigated, but DOX encapsulated liposomes targeting human epidermal growth factor receptor 2 (HER2) and EGFR are currently being evaluated.[40–42]

However, cellular uptake of the VNPs might reduce the efficiency of loaded protein therapeutics that have extracellular targets, such as TNF or IL-2. Thus, for optimal extracellular delivery at the TME the VNPs must be functionalized with targeting ligands that trigger low or no internalization of the nanoparticles. For instance, fibroblast activation protein-α (FAP) is overexpressed on cancer-associated fibroblasts in the tumor stroma and does not trigger ligand internalization.[43] Similarly, CD20 is a tetraspanin that has slow internalization kinetics and might be of use for tumor micro-environmental release. Due to the versatility of the VNP DDS, alternative biotinylated targeting moieties can be easily compared, and selected based upon minimized cellular internalization.

Of note, the gelatin shell of the VNP DDS not only provides functional groups for further functionalization but can also act as a second stimulus for controlled drug release. Specifically, gelatin can be degraded by matrix metalloproteinases (MMPs) that are overexpressed in the tumor microenvironment. Although not investigated here, this MMP sensitivity has been explored by several other groups for controlled drug release.[44–46] Thus, it would be of interest to study the targeting ability of, e.g., FAP functionalized VNPs, investigate the drug release at low pH present in the TME and in combination with MMPs, as well as nanoparticle internalization characteristics in vitro and in vivo.

4. Conclusion

In conclusion, we developed a versatile DDS for the controlled delivery of hydrophilic immunotherapeutic drugs using vaterite nanoparticles. The pH sensitivity of vaterite allows for the selective and controlled release of drugs at the acidic environment of the tumor. Further, the vaterite surface was engineered for an easy bioconjugation of targeting ligands by taking advantage of amine-epoxy click chemistry to equip the DDS with the streptavidin-biotin targeting system. Taken together, the proposed functionalized DDS can be of use in protein-based cancer immunotherapy or analogous applications.

5. Experimental Section

Recombinant Proteins, Reagents, and Materials: TNF was a kind gift from Prof. Dr. Harald Wajant, University of Wuerzburg, (Wuerzburg, Germany). Tris(hydroxymethyl)aminomethane (1.08382) and Na_2CO_3 (1.06392) were obtained from Merck (Germany, Darmstadt). Triton X-100 (X100), Poly(Ethylene Glycol) (500 kDa) Diglycidyl Ether (475 696), $NaHCO_3$ (S5761), ethylene glycol (EG, 102 466), HEPES (H4034), Tetramethylrhodamine isothiocyanate (TRITC, 283 924), Glutaraldehyde (49 629), and Gelatin A (G2500) were purchased from Sigma Aldrich (United States, Saint Louis). Gelatin B (PN 241 377) was purchased from GELITA (Germany, Eberbach). Streptavidin–FITC (434 311) was obtained from ThermoFisher Scientific (United States, Waltham). Poly(Ethylene Glycol) (400 kDa) Diglycidyl Ether (0 8210), and Glycidyl Glycerol-Ether, Polyfunctional (0 9221) were acquired from Polysciences Europe (Germany, Hirschberg an der Bergstrasse). Incucyte CytoLight Rapid Red (4706) was purchased from Essen Bioscience (Sartorius, Germany, Göttingen). In-house labeling of proteins was done with TRITC. MilliQ was generated using PURELAB classic from ELGA (United Kingdom, High Wycombe). Phosphate buffered saline (PBS) was purchased from Apotheek A15 (EP00398, Netherlands, Gorinchem). Samples were centrifuged with an Eppendorf centrifuge (5427R, Germany, Hamburg).

Synthesis of Vaterite Nanoparticles (VNP): VNPs were prepared as previously described.[21] Briefly, 5 mL $CaCl_2{\cdot}2H_2O$ (0.33 M, 80% EG) was added to a 25 mL beaker and stirred at 1300 rpm (Cimarec+, SP88857105, ThermoFisher Scientific, United States, Waltham), then 5 mL $NaHCO_3$ (0.33 M in 80% EG) was quickly added and incubated under stirring for 2 h at room temperature (RT). The VNPs were subsequently centrifuged to remove EG (10 000 g, 10 min) and washed three times with water (3000 g, 5 min) and one time with ethanol (3000 g, 5 min) and dried at 60 °C overnight.

TNF Loading to VNPs (VNP-TNF): Ten milligrams of dried VNPs were dispersed in HEPES buffer (0.1 M, pH 7.5) with ultrasonication (Soniprep 150, MSE), after which TNF was added to a final concentration of 0.25 mg mL^{-1} in 500 µL buffer. The particles were incubated under rotation for 1 h at RT, then washed two times with MilliQ (3000 g, 2 min) and stored at −20 °C until further use.

Gelatin Coating of Vaterite Nanoparticles and Cross-Linking to Streptavidin (VNP-TNF-Gel-Strep): Five milligrams of VNP-TNF was added to 500 µL gelatin A or B solution (2% in 0.1 M HEPES pH 8.0) and incubated at 37 °C under shaking (1000 rpm, Bioshake iQ, QINSTRUMENTS, Germany, Jena)

for 30 min, followed by two washes (3000 g, 5 min) with HEPES buffer. Particles were stored at −20 °C until further use. Streptavidin was coupled to the gelatin coating on the VNP through an amine-epoxy reaction. In brief, 5 mg of particles was dispersed in HEPES buffer (150 mM, pH 8.5) then different glycidyl-bearing epoxy moieties, indicated in the figures, were added at a final concentration of 0.1 mg mL^{-1} together with 0.2 mg mL^{-1} streptavidin and incubated at 37 °C for 6 h under shaking (1000 rpm, Bioshake iQ, QINSTRUMENTS, Germany, Jena). Glutaraldehyde was also employed as a cross-linker with a final concentration of 0.1% for 30 min at RT. The particles were then washed twice with HEPES buffer (3000 g, 3 min) and stored at −20 °C.

Confocal Microscopy of Gelatin B Coated VNP: Five milligrams of VNPs coated with rhodamine labelled Gelatin B (VNP-GelB-Rhodamine) were resuspended in ethanol and diluted in ethanol to 0.05 mg mL^{-1}. Ten microliters of the diluted VNP-GelB-Rhodamine was added to a microscopy slide and left to dry, followed by imaging with the Leica SP8X DLS with a HC PL APO CS2 63x/1.4 oil objective.

Antibody Biotinylation and Binding to Streptavidin Functionalized VNPs: CTX and RTX labeling with biotin was performed following manufacturer protocol (20 217, ThermoFisher Scientific, United States, Waltham,). In brief, 2 mg CTX or RTX was dissolved in 1 mL HEPES buffer (pH 8.5) then 26.6 µL biotin was added (10 mM in DMSO) and incubated at RT under shaking (1000 rpm, Bioshake iQ, QINSTRUMENTS, Germany, Jena) for 30 min. The labelled protein was purified using Ultra Centrifugal Filter Units with 10K MWCO (UFC501024, MERCK, Germany, Darmstadt) (14 000 g, 15 min) and restored in HEPES buffer at 4 °C.

Biolayer Interferometry Analysis of CTX-Biotin to EGFR: Binding of CTX-biotin to His-EGFR (cat# Z03194, GenScript, Rijswijk, the Netherlands) was analyzed using the BLItz system from ForteBio (cat# 45–5000, ForteBio, Menlo Park, CA, USA). Octet HIS1K biosensors (cat# 18–5120, Satorius, Göttingen, Germany) were wetted for at least 10 min before use in PBS and all samples were diluted in the same buffer. In short, a baseline was run for 30 s, followed by loading of 10 µg mL^{-1} (≈125 nM) of EGFR-his for 120 s, baseline for 30 s, association of 2 µg mL^{-1} CTX-biotin for 120 s, and dissociation for 120 s. RTX (30 µg mL^{-1}) was used as a control. Step corrections were applied to both the start of association and dissociation. Finally, the individual experiments were aligned to the start of association (x = y = 0 for t = 180 s).

Antibody Coupling to the Surface of VNP-TNF-Gel-Strep: Two milligrams of VNP-TNF-Gel-Strep was dispersed in 200 µL HEPES pH 8.0 then 10 µL of CTX-Biotin (4 mg mL^{-1}) or 20 µL of RTX-biotin (2 mg mL^{-1}) was added and incubated under shaking (1000 rpm, Bioshake iQ, QINSTRUMENTS, Germany, Jena) at RT for 40 min. The particles were then washed with HEPES buffer (3000 g, 2 min) and stored at −20 °C until further use.

Particle Characterization: The morphological characterization of VNPs was performed using a field emission scanning electron microscope (FESEM, Zeiss Supra 40VP, Germany, Jena). The size distribution was determined by Disc centrifuge (CPS Instruments, Inc., United States, Prairieville) and Zeta-potential was evaluated using a MALVERN Zeta Potential/Particle Sizer (Model ZEN5600, United Kingdom, Malvern).

Cell Lines and Cell Culture: FaDu, Daudi, SU-DHL-2, SU-DHL-4, SUD-HL-6, SUD-HL-10, SC1, RI1, OCI-LY3, and U-2932 were obtained from the American Type Culture Collection (ATCC, United States, Manassas). Cell lines were cultured at 37 °C, in a humidified 5% CO_2 atmosphere in DMEM or RPMI (Biowhittaker BE12–604F and BE12–155F, Lonza, Switzerland, Basel) supplemented with 10% fetal calf serum (FCS) (F7524, Sigma Aldrich, United States, Saint Louis).

ICAM-1 Expression: FaDu cells (4×10^4/well) were pre-seeded in a 96 well plate (167 008, ThermoFisher Scientific, United States, Waltham) in DMEM 10% FCS and allowed to adhere. Vaterite nanoparticles were added to each well as indicated (10 µg in all conditions) and incubated overnight. FaDu cells were washed, detached using 1x trypsin-EDTA (59418C, Sigma Aldrich, United States, Saint Louis), transferred to FACS tubes, and stained with anti-ICAM-1-APC (21 279 546, ImmunoTools, Germany, Friesoythe) for 1 h on ice. Subsequently, the stained cells were washed with PBS then analyzed by CytoFLEX flow cytometer (A00-1-1102, Beckman Coulter, United states, Indianapolis). ICAM-1 fold increase was calculated as the MFI of treated FaDu divided by the MFI of untreated control FaDu. Alternatively, vaterite nanoparticles were first added to full medium at pH 7.4 or 5.0 and incubated overnight (10 µg in all conditions), followed by centrifugation (3000 g, 5 min). The supernatant was then added to FaDu cells, and the protocol was followed, as mentioned above.

VNP-Streptavidin Binding to Biotinylated Cells: To verify the functional activity of Strep-VNP, Daudi, SU-DHL-2, SU-DHL-4, SUD-HL-6, SUD-HL-10, SC1, RI1, OCI-LY3, and U-2932 cells (10×10^4/FACS tube, in RPMI 10% FCS) were treated with 5 µg mL^{-1} RTX for 1 h on ice then washed twice with PBS (3000 g, 3 min). Subsequently, cells were resuspended in 200 µL RPMI and treated with 4 µL anti-Human IgG1 Fc-Biotin (1 mg mL^{-1}, ThermoFisher Scientific, United States, Waltham) for 1 h on ice, then washed twice with PBS (3000 g, 3 min) and treated with VNP-TNF-GelB-Strep (50 µg mL^{-1}) for 1 h at 4 °C under rotation (50 rpm, PTR-60, Grant Bio, United Kingdom, Shepreth). All groups were then washed with PBS and surface-bound nanoparticles were detected as a function of FITC positive cells by flow cytometry (CytoFLEX).

VNP-CTX and VNP-RTX Binding Assay: Cells (10×10^4/FACS tube) in DMEM/RPMI 10% FCS were treated with 50 µg mL^{-1} VNP-CTX/RTX for 1 h at 4 °C under rotation (50 rpm, PTR-60, Grant Bio, United Kingdom, Shepreth). The excess of particles was removed by washing cells with PBS (3000 g, 3 min) then surface bound VNP-CTX/RTX were measured using flow cytometry (CytoFLEX). The binding of VNP-CTX in mix culture of FaDu and Daudi was performed similarly.

Cellular Uptake of VNPs by FaDu Cells: Hundred microliters of 1×10^4 FaDu cells in DMEM 10% FCS stained with Incucyte Red were plated in a 96-wells plate and incubated overnight. Then 0.1 mg mL^{-1} of FITC-labeled VNP-CTX, VNP-RTX, or VNP were added, and particle uptake was followed using Incucyte S3 (Sartorius, Germany, Göttingen) by imaging every hour for 24 h at 37 °C with 5% CO_2. Images were processed using Incucyte's basic analyzer using a segmentation surface fit with a threshold (GCU) of 0.1 with edge split on for the green channel (VNP) and a threshold (RCU) of 0.25 with edge split off and hole fill of 50 μm^2 for the red channel (FaDu). The integrated VNP intensity was divided by the total area of FaDu cells and normalized to hour zero. Finally, the background intensity of the control (FaDu only) was subtracted from the results.

VNP Uptake in FaDu Cells by Confocal Microscopy: VNP uptake was imaged with the Zeiss cell discoverer 7 (Germany, Jena). Hereto, 300 µL of 3×10^4 FaDu cells in DMEM 10% FCS were seeded in an 8-well borosilicate slide (Nunc Lab-Tek II Chambered coverglass, 154 461, ThermoFisher Scientific, United States, Waltham) and incubated overnight. The next day, 0.1 mg mL^{-1} of FITC labeled VNP-GelB-Strep, VNP-CTX or Rhodamine labeled VNP-GelB were added and incubated overnight. Next morning, anti-CD47 antibody (FITC 21 270 473, ImmunoTools, Germany, Friesoythe or APC 323 124, Biolegend, United States, San Diego) was added 15 min before image acquisition and cells were washed thrice with full medium. Cells and particles were imaged live with the cell discoverer 7 using a PlanApochromat 50x/1.2 water (WD = 0.84 mm) objective in combination with a 0.5x optovar lens and a LSM900 confocal head at 37 °C with 5% CO_2. Diode lasers (488 and 561) were used to detect FITC (VNP or CD47), Rhodamine (VNP-GelB) or APC (CD47) signal using an Airyscan2 detector. All image processing was performed using ZEN blue (V3.5) software.

Jurkat.NFκB.Luciferase Assay: Jurkat cells were electroporated (Amaxa nucleofector I, Lonza, Switzerland, Basel) with the pNL3.2.NF-κB-RE [NlucP/NF-κB-RE/Hygro] Vector (N111A, Promega, United States, Wisconsin) according to manufacturer's protocol (VCA-1003, Amaxa cell line nucleofector Kit V, Lonza, Switzerland, Basel) and grown in RPMI, supplemented with 10% FCS and 500 µg mL^{-1} Hygromycin B (10 687 010, ThermoFisher Scientific, United States, Waltham), creating the Jurkat.NFκB.Luciferase cell line. Hundred microliters containing 5×10^4 cells were incubated for 6 h at 37 °C in a 96-well plate (3917, Corning 96-well Solid White Flat Bottom, United States, Corning) with particles (0.1 mg mL^{-1}) or the supernatant of particles (0.1 mg mL^{-1}) released overnight in RPMI with 10% FCS, adjusted to pH 5 or pH 7. After incubation the luminescence was measured using a luminescence reader (Synergy, BioTek, United States, Winooski) by addition of 30 µL of Nano-Glo Luciferase Assay System (N1110, Promega, United States, Wisconsin,) and incubation of 10 min. Data was acquired using Gen5 (V2.03)

software at 37 °C (emission:hole, optics:top, gain:auto, integration time:1 s, read height: 1 mm). The fold change was calculated as follows:

$$Fold\ change = \frac{[sample\ luminescence] - [control\ luminescence]}{[control\ luminescence]} \quad (1)$$

With control luminescence defined as untreated Jurkat.NFκB.Luciferase cells.

Viability Assay: FaDu cells (5×10^3) were pre-plated in a 96-well plate (DMEM 10% FCS). After 24 h, fresh medium containing 0.1 mg mL^{-1} of VNP-GelB was added followed by an overnight incubation. The next morning, the medium was aspirated and either the cells were trypsinized using TrypLE (12 604 013, ThermoFisher Scientific, United States, Waltham), stained for Annexin V (APC 640 941, Biolegend, United States, San Diego)/PI (P3566, Invitrogen, United States, Waltham) in 1x calcium buffer (556 454, BD Biosciences, Germany, Heidelberg) and measured by flow cytometry (CytoFLEX), with viability defined as percentage of double negative (AnV-/PI-) cells. Or the cells were washed twice with fresh medium, 15 µL MTS+PMS (G5421, Promega, United States, Wisconsin) was added to 100 µL fresh medium and the absorbance was measured at 490 nm (51119600DP, multiscan sky, ThermoFisher Scientific, United States, Waltham), after ≈2 h. As negative control 15 µL of 10% Triton X-100 in 70% ethanol was first added to untreated FaDu cells, followed by MTS, as described above. The obtained absorbance was normalized by defining 0% as the smallest and 100% as the largest mean in each data set (dead, control, VNP-GelB).

TNF Loading Capacity and Weight Determination by ELISA: Different VNPs (0.1 mg) were dissolved in 100 mM acetate buffer pH 5.0 to release TNF, prior to the ELISA assay. The TNF concentration was determined by a TNF ELISA kit (31 673 019, ImmunoTools, Germany, Friesoythe), according to manufacturer's protocol, with the exception that all samples and standards were prepared in acetate buffer instead of PBS. The percentile loss of TNF between each step was calculated as follows:

$$TNF\ loss\ \ (\%) = 100 - \left(\frac{[TNF\ weight\ current\ step]}{[TNF\ weight\ previous\ step]} * 100\right) \quad (2)$$

The loading capacity of TNF was calculated as follows:

$$Loading\ capcity\ \ (\%) = \left(\frac{[TNF\ weight]}{[TNF\ weight + VNP\ weight]} * 100\right) \quad (3)$$

Data and Statistical Analysis: Data was plotted using GraphPad Prism Software (V9.1.0) and represented as mean ± SD of three independent experiments. Data was analyzed using an unpaired Student's T-test (in case of two samples) or one-way ANOVA followed by the Tukey Kramer post-test. A P value < 0.05 was considered statistically significant. Flow cytometry data was plotted using FlowJo Software (V10.8.1).

Supporting Information

Supporting Information is available from the Wiley Online Library or from the author.

Acknowledgements

L.C.N. and G.C. contributed equally to this work and share first authorship. This research was funded by the European Union under the Marie Sklodowska-Curie grant agreement No 813871 and Stichting de Cock-Hadders grant number 67663. The authors would like to thank Lisa Jakob for performing the experiments for the revisions.

Conflict of Interest

The authors declare no conflict of interest.

Data Availability Statement

The data that support the findings of this study are available from the corresponding author upon reasonable request.

Keywords

calcium carbonate, vaterite, nanoparticles, protein encapsulation, active targeting, controlled release

Received: October 6, 2023
Revised: February 22, 2024
Published online: March 12, 2024

[1] B. A. Wilky, *Immunol. Rev.* **2019**, *290*, 6.
[2] J. J. Havel, D. Chowell, T. A. Chan, *Nat. Rev. Cancer* **2019**, *19*, 133.
[3] L. B. Kennedy, A. K. S. Salama, *CA Cancer J. Clin.* **2020**, *70*, 86.
[4] J. A. Thompson, *J. Natl. Compr. Cancer Network* **2018**, *16*, 594.
[5] L. Da, Y. Teng, N. Wang, K. Zaguirre, Y. Liu, Y. Qi, F. Song, *Front. Pharmacol.* **2019**, *10*, 1671.
[6] A. M. Zeidan, D. J. DeAngelo, J. Palmer, C. S. Seet, M. S. Tallman, X. Wei, H. Raymon, P. Sriraman, S. Kopytek, J. P. Bewersdorf, M. R. Burgess, K. Hege, W. Stock, *Ann. Hematol.* **2022**, *101*, 557.
[7] C. Krieg, S. Letourneau, G. Pantaleo, O. Boyman, *Proc. Natl. Acad. Sci. USA* **2010**, *107*, 11906.
[8] J. L. Abbruzzese, B. Levin, J. A. Ajani, J. S. Faintuch, S. Saks, Y. Z. Patt, C. Edwards, K. Ende, J. U. Gutterman, *Cancer Res.* **1989**, *49*, 4057.
[9] M. Blick, S. A. Sherwin, M. Rosenblum, J. Gutterman, *Cancer Res.* **1987**, *47*, 2986.
[10] C. Verhoef, J. H. de Wilt, D. J. Grunhagen, A. N. van Geel, T. L. ten Hagen, A. M. Eggermont, *Curr. Treat. Options Oncol.* **2007**, *8*, 417.
[11] S. Bonvalot, F. Rimareix, S. Causeret, C. L.e Pechoux, B. Boulet, P. Terrier, A. Le Cesne, J. Muret, *Ann. Surg. Oncol.* **2009**, *16*, 3350.
[12] S. D. Jo, G.-H. Nam, G. Kwak, Y. Yang, I. C. Kwon, *Nano Today* **2017**, *17*, 23.
[13] K. Shao, S. Singha, X. Clemente-Casares, S. Tsai, Y. Yang, P. Santamaria, *ACS Nano* **2015**, *9*, 16.
[14] P. Velpurisiva, A. Gad, B. Piel, R. Jadia, P. Rai, *J. Biomed.* **2017**, *2*, 64.
[15] R. Toy, K. Roy, *Bioeng. Transl. Med.* **2016**, *1*, 47.
[16] K. Li, D. Li, L. Zhao, Y. Chang, Y. Zhang, Y. Cui, Z. Zhang, *Bioact. Mater.* **2020**, *5*, 721.
[17] A. Sergeeva, R. Sergeev, E. Lengert, A. Zakharevich, B. Parakhonskiy, D. Gorin, S. Sergeev, D. Volodkin, *ACS Appl. Mater. Interfaces* **2015**, *7*, 21315.
[18] Y. Tarakanchikova, A. Muslimov, I. Sergeev, K. Lepik, N. Yolshin, A. Goncharenko, K. Vasilyev, I. Eliseev, A. Bukatin, V. Sergeev, S. Pavlov, A. Popov, I. Meglinski, B. Afanasiev, B. Parakhonskiy, G. Sukhorukov, D. Gorin, *J. Mater. Chem. B* **2020**, *8*, 9576.
[19] N. A. Feoktistova, A. S. Vikulina, N. G. Balabushevich, A. G. Skirtach, D. Volodkin, *Mater. Des.* **2020**, *185*, 108223.
[20] G. Choukrani, J. Álvarez Freile, N. U. Avtenyuk, W. Wan, K. Zimmermann, E. Bremer, L. Dähne, *Part. Part. Syst. Charact.* **2021**, *38*, 2100012.
[21] B. V. Parakhonskiy, A. Haase, R. Antolini, *Angew. Chem., Int. Ed. Engl.* **2012**, *51*, 1195.
[22] A. Burke-Gaffney, P. G. Hellewell, *Br. J. Pharmacol.* **1996**, *119*, 1149.
[23] M. J. Glennie, R. R. French, M. S. Cragg, R. P. Taylor, *Mol. Immunol.* **2007**, *44*, 3823.
[24] F. Céspedes, S. Alegret, *TrAC Trends Anal. Chem.* **2000**, *19*, 276.
[25] M. E. Tess, J. A. Cox, *J. Pharm. Biomed. Anal.* **1999**, *19*, 55.

[26] M. C. Stuparu, A. Khan, in *Click Polymerization*, (Eds: A. Qin, B. Z. Tang), The Royal Society of Chemistry, Cambridge, United Kingdom **2018**, p. 191.
[27] Z. Wang, Y. Chen, S. Chen, F. Chu, R. Zhang, Y. Wang, D. Fan, *RSC Adv.* **2019**, *9*, 35273.
[28] T. Iype, J. Thomas, S. Mohan, K. K. Johnson, L. E. George, L. A. Ambattu, A. Bhati, K. Ailsworth, B. Menon, S. M. Rayabandla, R. A. Jesudasan, S. Santhosh, C. N. Ramchand, *Anal. Biochem.* **2017**, *519*, 42.
[29] F. Alexis, E. Pridgen, L. K. Molnar, O. C. Farokhzad, *Mol. Pharm.* **2008**, *5*, 505.
[30] K. Yumura, M. Ui, H. Doi, T. Hamakubo, T. Kodama, K. Tsumoto, A. Sugiyama, *Protein Sci.* **2013**, *22*, 213.
[31] D. L. Meyer, J. Schultz, Y. Lin, A. Henry, J. Sanderson, J. M. Jackson, S. Goshorn, A. R. Rees, S. S. Graves, *Protein Sci.* **2001**, *10*, 491.
[32] T. Kawato, E. Mizohata, T. Meshizuka, H. Doi, T. Kawamura, H. Matsumura, K. Yumura, K. Tsumoto, T. Kodama, T. Inoue, A. Sugiyama, *J. Biosci. Bioeng.* **2015**, *119*, 642.
[33] P. Martin-Killias, N. Stefan, S. Rothschild, A. Pluckthun, U. Zangemeister-Wittke, *Clin. Cancer Res.* **2011**, *17*, 100.
[34] M. Simon, U. Zangemeister-Wittke, A. Pluckthun, *Bioconjug. Chem.* **2012**, *23*, 279.
[35] R. Tamaskovic, M. Simon, N. Stefan, M. Schwill, A. Pluckthun, *Methods Enzymol.* **2012**, *503*, 101.
[36] S. K. Blick, L. J. Scott, *Drugs* **2007**, *67*, 2585.
[37] M. P. Morelli, T. Cascone, T. Troiani, C. Tuccillo, R. Bianco, N. Normanno, M. Romano, B. M. Veneziani, G. Fontanini, S. G. Eckhardt, S. De Pacido, G. Tortora, F. Ciardiello, *J. Cell. Physiol.* **2006**, *208*, 344.
[38] C. Tan, C. Dima, M. Huang, E. Assadpour, J. Wang, B. Sun, M. S. Kharazmi, S. M. Jafari, *Adv. Colloid Interface Sci.* **2022**, *309*, 102791.
[39] Y. Zhao, Z. Luo, M. Li, Q. Qu, X. Ma, S. H. Yu, Y. Zhao, *Angew. Chem., Int. Ed. Engl.* **2015**, *54*, 919.
[40] K. M. Laginha, E. H. Moase, N. Yu, A. Huang, T. M. Allen, *J. Drug Targeting* **2008**, *16*, 605.
[41] B. Kasenda, D. Konig, M. Manni, R. Ritschard, U. Duthaler, E. Bartoszek, A. Barenwaldt, S. Deuster, G. Hutter, D. Cordier, L. Mariani, J. Hench, S. Frank, S. Krahenbuhl, A. Zippelius, C. Rochlitz, C. Mamot, A. Wicki, H. Laubli, *ESMO Open* **2022**, *7*, 100365.
[42] C. Mamot, R. Ritschard, A. Wicki, G. Stehle, T. Dieterle, L. Bubendorf, C. Hilker, S. Deuster, R. Herrmann, C. Rochlitz, *Lancet Oncol.* **2012**, *13*, 1234.
[43] L. Xin, J. Gao, Z. Zheng, Y. Chen, S. Lv, Z. Zhao, C. Yu, X. Yang, R. Zhang, *Front. Oncol.* **2021**, *11*, 648187.
[44] L. J. McCawley, L. M. Matrisian, *Mol. Med. Today* **2000**, *6*, 149.
[45] K. Vaghasiya, E. Ray, A. Sharma, O. P. Katare, R. K. Verma, *ACS Appl. Bio Mater.* **2020**, *3*, 4987.
[46] H. Li, S. S. Yu, M. Miteva, C. E. Nelson, T. Werfel, T. D. Giorgio, C. L. Duvall, *Adv. Funct. Mater.* **2013**, *23*, 3040.

